High PD-1/PD-L1 checkpoint interaction infers tumour selection and therapeutic sensitivity to anti-PD1/PD-L1 treatment

Lissete Sánchez-Magraner[1**], James Miles[1,2,3,10**], Claire Baker[2], Christopher J Applebee[1,2,3], Dae-Jin Lee[4], Somaia Elsheikh[5], Shaimaa Lashin[5], Katriona Withers[2], Andrew Watts[6], Richard Parry[6], Christine Edmead[3,7], Jose Ignacio Lopez[8], Raj Mehta[9] , Antoine Italiano[10], Stephen G Ward[7], Peter J. Parker*[11,12], Banafshé Larijani*[1,2,3]

[1]FASTBASE Solutions S.L, Astondo bidea, Kabi 612 Scientific and Technology Park of Bizkaia 48160 Derio, Spain
[2]Cell Biophysics Laboratory, Ikerbasque, Basque Foundation for Science, Research Centre for Experimental Marine Biology and Biotechnology (PiE) & Biophysics Institute (UPV/EHU, CSIC), University of the Basque Country, Spain.
[3]Centre for Therapeutic Innovation, Cell Biophysics Laboratory, Department of Pharmacy and Pharmacology, & Department of Physics, University of Bath, Claverton Down, Bath, BA2 7AY United Kingdom
[4]Basque Centre for Applied Mathematics, Alameda de Mazarredo 14, Bilbao, Bizkaia, 48009, Spain
[5]Department of Cellular Pathology, Queens Medical Centre, Nottingham, NG7 2UH, United Kingdom
[6]Bath ASU, 3 Corsham Science Park, Park Lane, Corsham SN13 9FU, United Kingdom
[7]Leukocyte Biology Laboratory, Centre for Therapeutic Innovation & Department of Pharmacy and Pharmacology, University of Bath, Claverton Down, Bath BA2 7AY United Kingdom
[8]Department of Pathology, Cruces University Hospital, Biocruces Research Institute, Barakaldo, Bizkaia, 48903, Spain
[9]Gamma Delta Therapeutics Ltd., London Bioscience Innovation Centre, London, NW1 0NH, United Kingdom.
[10]Early Phase Trials and Sarcoma, Institut Bergonié, Cours de l'Argonne, Bordeaux, France, 33000, France
[11]Protein Phosphorylation Laboratory, The Francis Crick Institute, London, NW1 1AT United Kingdom.
[12]School of Cancer and Pharmaceutical Sciences, King's College London, London, WC2R 2LS, United Kingdom.

** Equal First author contribution
*Corresponding Authors:

Professor Peter J Parker,
Protein Phosphorylation Laboratory,
The Francis Crick Institute,
1 Midland Road,
London,
NW1 1AT,
peter.parker@crick.ac.uk,
+44 (0)20 3796 1977

Professor Banafshé Larijani,
Centre for Therapeutic Innovation,
Department of Pharmacy and Pharmacology,
University of Bath,
Claverton Down,
Bath,
BA2 7AY,
bl666@bath.ac.uk,
+44 (0) 1225 384040

Running Title

Therapeutic sensitivity to PD-1 & PD-L1 interaction

Abbreviations

PD-1: Programmed death receptor-1

PD-L1: Programmed death-ligand 1

CTLA-4: Cytotoxic T-lymphocyte-associated protein 4

CD80: Cluster of differentiation 80

FRET: Förster resonance energy transfer

FLIM: Fluorescence lifetime imaging microscopy

ccRCC: clear cell renal cell carcinoma

MSTS: multi-site tumour sampling

H&E: haematoxylin and eosin

NSCLC: Non-small-cell lung cancer

Disclosure: BL and PJP are cofounders of FASTBASE Solutions S.

Abstract

Many cancers are termed immuno-evasive due to expression of immuno-modulatory ligands. Programmed death ligand-1 (PD-L1) and cluster of differentiation 80/86 (CD80/86) interact with their receptors, (programmed death receptor-1 (PD-1) and cytotoxic T-lymphocyte associated protein-4 (CTLA-4) respectively), on tumour infiltrating leukocytes, thus eliciting immunosuppression. Immunotherapies aimed at blocking these interactions are revolutionising cancer treatments, albeit in an inadequately described patient subset. To address the issue of patient stratification for immune checkpoint intervention, we have quantitatively imaged PD-1/PD-L1 interactions in tumour samples from patients, employing an assay that readily detects these intercellular protein-protein interactions in the ≤10nm range. These analyses across multiple patient cohorts demonstrate the inter-cancer, inter-patient and intra-tumoural heterogeneity of interacting immune-checkpoints. We have shown that PD-1/PD-L1 interaction is not correlated with clinical PD-L1 expression scores in malignant melanoma. Crucially, amongst anti-PD-1 treated metastatic NSCLC patients, those with lower PD-1/PD-L1 interaction have significantly worsened survival. It is surmised that within tumours selecting for an elevated level of PD-1/PD-L1 interaction, there is a greater dependence on this pathway for immune evasion and hence they exhibit more impressive patient response to intervention.

Keywords: FRET-FLIM, Cancer, Immune-checkpoint, PD-1/PD-L1, CTLA-4/CD80 immunotherapy.

Statement of Significance

Contrary to current studies, quantitation of immune-checkpoint interaction by direct imaging, demonstrates that, immunotherapy treated patients with metastatic non-small-cell lung cancer, with a low extent of PD-1/PD-L1 interaction, show significantly worse outcome.

Introduction

Disproportionate immune-system activation can result in profound pathologies and there are therefore regulatory mechanisms in place to maintain homeostasis (1). Interactions referred to as immune-checkpoints are critical in this, avoiding immune-cell related collateral damage in pathogenic responses and in suppressing autoimmunity. Inhibitory receptors presented by immune cells, T-cells in particular, include programmed death receptor-1 (PD-1) and cytotoxic T lymphocyte antigen-4 (CTLA-4) (2,3). Cancers exploit these physiological mechanisms to avoid immune-attack by expressing inhibitory receptor cognate ligands, programmed death-ligand 1 (PD-L1) and cluster of differentiation 80/86 (CD80/86) (1). The CTLA-4 receptor is a homolog of the immune-activating CD28 receptor, both of which are found on T-cells and possess CD80 and CD86 as ligand partners (4). CTLA-4, however, provides a higher affinity binding site for CD80/86 and interaction with CD80/86 inhibits cell proliferation and interleukin-2 (IL-2) secretion by T-cells. The PD-1 immune checkpoint, limits later immune responses primarily in peripheral tissue by attenuating T-cell signalling downstream of the T-cell receptor (5).

There are a number of approved therapeutic monoclonal antibodies (mAbs) designed to reinstate immune-mediated tumour destruction in immunogenic cancers, by inhibiting the aforementioned immune-checkpoint interactions (6). In part through the generation of neo-antigens, immunogenicity is strong in non-small-cell-lung-cancer (NSCLC), renal cell carcinomas (RCCs), melanoma, classical Hodgkin lymphoma, head and neck squamous cell carcinoma and

urothelial carcinoma, all of which show varying degrees of response to immune-checkpoint interventions (6-8). Notwithstanding some remarkable successes with immune-checkpoint inhibitors, the majority of patients display primary or acquired resistance to treatment (9). There is therefore an unmet clinical need to identify biomarkers that distinguish potential responders from non-responders to ensure that non-responders are not exposed to the side effects of these drugs for no therapeutic benefit.

The development of different PD-L1 immunohistochemistry (IHC) diagnostics utilising proprietary antibodies has resulted in four FDA-approved and CE-*in vitro* diagnostics (IVD)-marked assays, each linked to a specific drug and scoring system (10). However, it has become clear that the expression of inhibitory ligands, namely PD-L1, are not an accurate diagnostic marker for use in predicting patient prognosis and response to treatment. A recent study observed that NSCLC patients demonstrated an increase in response to the anti-PD-1 agent, pembrolizumab, in patients exhibiting a tumour proportion score (TPS) greater than 50% (11). Nevertheless, the response reached only 41% (12). Moreover, a different study assessed the efficacy of PD-1 or PD-L1 inhibitors in different neoplasia (primarily lung cancer but also renal cancer and malignant melanoma) in PD-L1 negative and PD-L1 positive cancers. Critically, benefit was seen in patients within the PD-L1 negative group, clearly exposing the failure of PD-L1 expression to determine which patients should receive immune-checkpoint inhibitors (13).

As immune-cell/tumour-cell interplay via immune-checkpoints is a prominent mechanism for tumour immune-evasion and survival, checkpoint interaction status may present a key mechanism-based prognostic and/or predictive biomarker, replacing conventional protein expression readouts for stratifying patients to immune-checkpoint interventions. To this end we have developed and tested an imaging assay that provides a quantitative readout of immune-checkpoint interaction between cells. iFRET (immune-FRET), employs a two-site, cell-cell amplified Förster Resonance Energy Transfer method, detected by Fluorescence Lifetime Imaging Microscopy (FRET/FLIM). Here, iFRET acts as a “chemical ruler”, measuring cell-cell interactions in the range of 1-10nm. Alternative assays have assessed the PD-1/PD-L1signalling axis in both cell assays and patient tissue, however these assays work at a distance greater than that of iFRET (Supplementary Figure 1A). Work carried out by Giraldo et al., 2018 uses an imaging algorithm which determines when PD-1^+ and PD-$L1^+$ cells are within close proximity (≤20 μm) of each other. Such assays investigate distances that reflect proximity over interaction (14). Johnson et al., 2018 also utilise an Automated Quantitative Analysis platform which again maps cells based on PD-1 and PD-L1 expression profiles. In these assays the colocalization of PD-1 and PD-L1 expressing cells (i.e. μm range) is assumed to be an interaction state (15). Here, the intrinsic distance constraints of iFRET informs on interaction states as receptor and ligand pairs within 1-10nm of each other; distances exceeding 10nm are considered to be non-interacting.

In this study we have investigated the application of iFRET in formalin fixed paraffin embedded (FFPE) patient tumour biopsies to

assess checkpoint interaction, to understand the relationship of this to ligand expression and to judge the predictive power of the data in respect of patient response to immune checkpoint interventions.

Material and Methods

Pathology

ccRCC

Biopsies from clear cell renal cell carcinoma patients, diagnosed and treated at the Cruces University Hospital, Bizkaia, Spain, were graded and staged within the study. All patients gave written informed consent for the potential use of their resected tumours to be used for research. This study was approved by the Ethical and Scientific Committee (CEIC-Euskadi PI2015060). The International Society of Urological Pathology (ISUP) 2013 tumour grading system (16) was used to assign each sample using routine haematoxylin and eosin (H&E) staining. Tumours were graded and grouped as low (G1/2) and high (G3/4) grade for consistency. To assess PD-L1 expression, a multi-site tumour sampling (MSTS) method was used which samples more areas of a tumour with the aim of overcoming the problems of tissue heterogeneity (17). Samples were determined PD-L1 positive (>1%) or negative (<1%) using the Roche VENTANA PD-L1 (SP142) assay.

Malignant Melanoma

Cases of malignant melanoma (MM) used in this study were selected from all patients diagnosed with malignant melanoma between June 2003 and February 2017 at Nottingham University Hospital. The main selection criterion was tumours having a Breslow

thickness of >1mm. Patients gave written informed consent for their specimens to be stored and used for research. Patient clinicopathological data was obtained from Nottingham University Hospital PAS, WinPath and NotIS databases. Data and specimens were anonymised by using only their designated laboratory case reference. Ethical approval (ACP0000174) was gained from the Nottingham Health Science Biobank Access Committee. A cohort of 176 primary MM cases was used for iFRET analysis as tissue microarrays (TMAs). Within the TMA's, each patient had one tumour sample. Supplementary Table 2 summarises the clinical parameters of the 176 patients. Tumours were fully surgically excised, formalin-fixed and paraffin embedded (FFPE) in tissue blocks. Tissue cores of 1mm diameter were selected by studying haematoxylin and eosin stained sections most recently cut from the FFPE tissue block. The location of cores to remove from the tissue block were selected by scanning the slides and using Pannoramic Viewer software (3DHisTech). Cores were removed from the FFPE tissue blocks using the TMA Grand Master (3DHisTech) and arrayed into new paraffin blocks.

Metastatic NSCLC

Biopsies from 60 metastatic NSCLC tumours were obtained during interventional radiology procedures from Institut Bergonié (Supplementary Table 3). 36 patients were male and 24 female with a median age of 63 years (range 44-86 years). Performance status was defined with 50 patients given a performance status of ≤1 and 10 patients given a status of ≥1. Performance status is a measure of a patients progress with a grade of 0 being defined as fully active

with the patient being able to carry on all pre-disease activities without restriction. A score of 1-3 indicates increasing severity of limitations to daily activities and self-care. 4 is defined as completely disabled and 5 defined as dead (18). The clinical outcome of 40 patients who were treated with either nivolumab (n=37) or pembrolizumab (n=3) were provided and used for Kaplan-Meier survival analysis. Patients samples were collected between January 2014 and December 2017. This study was approved by the IRB of Institut Bergonié. Excised samples were formalin fixed and paraffin embedded (FFPE) in tissue blocks prior to being sliced and mounted on microscope slides. For iFRET analysis, three consecutive tissue slices of each patient's sample were provided. One slide for each patient was labelled with H&E and a trained pathologist (Jose Ignacio-Lopez) identified tumorous areas within the sample.

Antibodies and reagents

Monoclonal antibodies, mouse anti-PD-1 (catalogue number: ab52587, clone number: NAT105), rabbit anti-PD-L1 (catalogue number: ab205921, clone number: 28-8) and mouse anti-CTLA-4 (catalogue number: ab19792, clone number: BNI3) were purchased from Abcam. Rabbit anti-CD80 (catalogue number: MBS2522916, clone number: MEM-233) was purchased from MyBioSource. The experimental antibody J1201, which blocks PD-1/PD-L1 interactions was obtained from Promega. Ipilimumab, which blocks CTLA-4/CD-80 interactions was also obtained from Promega. Pierce endogenous peroxidase suppressor (35000), Signal Amplification kit (T20950) and Prolong diamond antifade mount (P36970) were obtained from Thermo Fisher Scientific. AffiniPure F(ab′)2 fragment donkey anti-mouse IgG and peroxidase-conjugated AffiniPure

F(ab′)2 fragment donkey anti-rabbit IgG were purchased from Jackson Immuno Research Laboratories. ATTO 488 NHS ester was purchased and was conjugated to the AffiniPure F(ab′)2 IgG as described by Veeriah et al. 2014 (19). Millicell® 8-well plates, (PEZGS0816) were purchased from Merck.

Time-resolved amplified immune-Förster resonance energy transfer (i-FRET) detected by fluorescence lifetime imaging microscopy (FLIM)

iFRET relies on a two-site labelling assay which is illustrated in Supplementary 1B. Briefly, two primary antibodies are used to detect the receptor and ligand respectively. These antibodies are then labelled with Fab fragments conjugated to the donor chromophore ATTO488 (for the receptor) and HRP for the ligand. Tyramide signal amplification is then use to label HRP with the acceptor chromophore, ALEXA594 (Supplementary Figure 2C). The conjugation of the chromophores to Fab fragments, which bind to the two primary antibodies, allows the critical FRET distance of 10 nm or less to be maintained and provided the appropriate tool for measuring cell-cell interactions. It should be noted that additional stains, such as DAPI cannot be added to iFRET samples as they disrupt the ability of ATTO488 and ALEXA594 to undergo FRET. Using a semi-automated, high throughput mfFLIM (FASTBASE Solutions S.L), a mapping file was created, which mapped each region of interest according to its position on the slide (Veeriah et al., 2014 (19)) (Supplementary Methods) . Phase lifetimes, average intensities and lifetime images were calculated automatically and translated to an excel spreadsheet. A decrease of donor lifetime (τD) in the presence of the acceptor chromophore (τDA) is indicative

of resonance energy transfer. FRET efficiency (E_f %) values were calculated using the following equation, where τD and τDA are the lifetimes of the donor in the absence and presence of the acceptor, respectively.

$$Ef(\%) = [1 - \left(\frac{\tau DA}{\tau D}\right)]x100$$

Due to the Förster radius (R_0) of the chromophore pair ATTO488 and Alexa594, the minimum distance that can exist between the chromophores is 5.83nm (Supplementary Figure 2B and Supplementary Methods). At this distance, energy transfer is maximal and yields a FRET efficiency of 50%.

Immune-FRET (iFRET) assay for PD-1/PD-L1 interaction in cell culture

The commercially validated Promega Blockade Bioassay, originally designed to measure the antibody blockade of PD-1/PD-L1 and CTLA-4/CD80 interaction by luminescence, was adapted for an i-FRET protocol with the aim of verifying the technique for detecting intercellular interaction of these ligand/receptor pairs. Cells were obtained from the Promega Blockade Bioassay and were screened for mycoplasma prior to dispatch. These cells were thawed and directly used in this assay only. PD-L1 expressing CHO-K1 cells were seeded onto Millicell® 8-well plates and were incubated at 37 °C with 5% CO_2 for 16 hours. The experimental blocking antibody J1201 (anti-PD-1) was added to 4 wells at 25µg/ml final concentration to inhibit receptor-ligand interaction. PD-1 expressing Jurkat cells were subsequently seeded in all wells and the plates were incubated for 20 hours at 37 °C with 5% CO_2. The unbound cells were removed and the plates washed three times for 5 minutes

with phosphate buffered saline (PBS) before being fixed with 4% paraformaldehyde (PFA) for 12 mins. The PFA was then removed and the plates were washed three times for 5 minutes with PBS. All samples were incubated with endogenous peroxidase suppressor for 30 minutes at room temperature before being washed with PBS. They were subsequently incubated with 1% (10mg/ml) Bovine Serum Albumin (BSA), for 1 hour at room temperature before a further three PBS washes.

Primary antibody staining was carried out by adding mouse anti-PD-1, (1:100 in BSA), the donor only (D) readout condition. Meanwhile the donor plus acceptor (D/A) readout condition was labelled with both anti-PD-1 (1:100) and rabbit anti-PD-L1 (1:500). The plate was incubated overnight at 4°C before being washed twice with PBS containing 0.02% Tween 20 (PBST). Secondary Fab fragments were added, the D wells were labelled with anti-mouse FabATTO488 (1:100) and the D/A wells labelled with FabATTO488 (1:100) and anti-rabbit FabHRP (1:200). The plate was then incubated for 2 hours at room temperature before being washed twice with PBST and once with PBS.

Tyramide signal amplification (TSA) was performed on the D/A wells for 20 minutes in the dark, via the addition of Alexa594-conjugated tyramide diluted in amplification buffer (1:100) in the presence of 0.15% H_2O_2 (Supplementary Figure 2C) (Veeriah et al., 2014 and Miles et al., 2017 (19,20)) The D/A wells were washed twice with PBST and once with PBS to remove the tyramide. 5µl of Prolong Diamond anti-fade mount was added per well before being mounted with a coverslip.

iFRET assay for CTLA-4/CD80 interaction in cell culture

CTLA-4 expressing Jurkat cells were first seeded onto Millicell® 8-well plate, before the blocking antibody ipilimumab (anti-CTLA-4) was added to 4 wells at 100µg/ml final concentration. The CD80 expressing Raji cells were subsequently seeded and the cells were incubated for 20 h at 37 °C with 5% CO_2. Unbound cells were removed by PBS washes. The cells were fixed, underwent endogenous peroxidase suppression and were blocked with BSA as described previously in the PD-1/PD-L1 cell assay. The primary antibodies were added; D wells were labelled with mouse monoclonal anti-CTLA-4 (1:100) and the D/A wells labelled with both anti-CTLA-4 (1:100) and rabbit polyclonal anti-CD80 (1:100). The rest of the protocol was conducted as described above for the PD-1/PD-L1 singe cell assay.

iFRET assay for PD-1/PD-L1 interaction in formalin fixed paraffin embedded clear cell renal cell carcinoma (ccRCC) tissue

Human ccRCC tissue samples were provided by Cruces University Hospital, Bizkaia, Spain. Consecutive cross sections of tissues were mounted on separate slides to allow D and D/A antibody labelling. Samples were from 22 patients, from which 5 consecutive tissue section slides were provided. Of the 5 samples, 2 were available for D and 2 for D/A staining, while the remaining section was analysed using H&E staining to determine regions of immune infiltration.

Immunohistochemistry with PD-L1 (SP-142, Ventana) was performed in Benchmark Ultra (Ventana) immunostainers following the specific protocol recommended by the manufacturer.

For iFRET sample preparation, antigen retrieval was carried out using Envision Flex solution pH9 and a PT-Link instrument (Dako), where the slides were heated to 95^{o}C for 20 minutes. Remaining paraffin was removed by PBS washes before containing tissue areas with a hydrophobic PAP pen border. 1-2 drops/slide of endogenous peroxidase suppressor were added and the slides were incubated in a humidified tray for 30 minutes at room temperature. The slides were then blocked with BSA and D slides labelled with anti-PD-1 while D/A slides were labelled with anti-PD-1 plus anti-PD-L1, following the previously described cell assay protocol.

iFRET assay for PD-1/PD-L1 interaction in formalin fixed paraffin embedded malignant melanoma TMAs

Human malignant melanoma TMAs were provided by Nottingham University Hospitals, United Kingdom. Consecutive cross sections of tissues were mounted on separate slides to allow D and D/A antibody labelling. Samples from 176 patients, with two consecutive tissue section slides per patient were provided. Of the two samples, one was available for D and one for D/A staining. The primary antibodies used were anti-PD-1 and anti-PD-L1 following the same protocol as the FFPE renal cell carcinoma tissue above.

iFRET assay for PD-1/PD-L1 interaction in formalin fixed paraffin embedded metastatic NSCLC

Human metastatic NSCLC tissue slices were provided by Institut Bergonié, France. Consecutive cross sections of tissues were mounted on separate slides to allow D and D/A antibody labelling. Samples from 40 patients, with two consecutive tissue section slides per patient were provided. Of the two samples, one was available for D and one for D/A staining. The primary antibodies used were anti-PD-1 and anti-PD-L1 following the same protocol as the FFPE ccRCC tissue above.

Statistical analysis

Statistical analysis and Box and Whisker plots were performed using Origin Pro8. Statistical differences were calculated between groups using the Mann-Whitney U test (values indicated on the Box and Whisker plots). The Mann-Whitney U test is a nonparametric test, thus not assuming a normal distribution of results. Box and Whisker plots represent the 25–75% (box) and the 1–99 (whiskers) ranges. Statistical differences are indicated with p values ≤0.05. Kaplan-Meier survival analysis was performed using SPSS. SPSS was also used to calculate Cox-Regression for Survival Analysis to assess which factors (age, sex, tumour stage, interaction state) were impacting overall survival. For NSCLC, patients were ranked in order of their FRET Efficiency (interaction status) and split into the two groups; those with the lowest 60% of median FRET efficiencies, and those with the highest 40%. For melanoma, patients were split into the highest 20% and lowest 80% of FRET efficiencies. To determine these cut-off points for melanoma and NSCLC patients, maximally selected rank statistics were performed using the R statistical software (version 3.6.2) and the maxstat (version 0.7-25)

package which provides several p-value approximations (21,22). Maximally selected rank statistics can be used for estimation as well as evaluation of a simple cut-point mode. The results provided by maxstat were consistent with the choice of bottom 80% and top 20% and 60% and 40% respectively. The log-rank (Mantel-Cox) test was carried out to determine significant differences between the groups.

Results

Development, validation and benchmarking of a novel amplified-FRET imaging assay for determining immune-checkpoint interaction in *ex vivo* assays

The iFRET assay used to measure immune-checkpoint interaction state is based on time-resolved FRET. Here, FRET acts as a “chemical ruler”, measuring distances of 1-10nm, which is the same order of magnitude as cell surface interactions. The maximum FRET efficiency value permitted is 50% (Supplementary Methods). Our definition of interaction are distances under 10nm, as opposed to PLA assays which detect distances of tens of nm and colocalization assays which range from 100nm up to 20 μm (Supplementary Figure 1) (14,23).

To develop and validate iFRET for the measurement of immune-checkpoint interactions, two antibodies (Promega) were employed; J1201, an experimental antibody for blocking PD-1/PD-L1 interactions, and ipilimumab for blocking CTLA-4/CD-80 interactions.

These antibodies were used to verify iFRET as a technique for detecting the intercellular interaction of these ligand/receptor pairs. These antibodies and cell lines were chosen as they were components from a commercially available validated assay.

Figure 1 illustrates the intercellular interaction of PD-1 and PD-L1, on Jurkat and CHO-K1 cells, using iFRET. Cells were not permeabilised and therefore the observable interaction was that of two membrane-bound, extracellular proteins. The FLIM images provided in the following figures consist of pseudocolour lifetime maps which represent lower lifetimes (red) and higher lifetimes (blue). Also provided are greyscale intensity maps which indicate donor (PD-1 or CTLA-4) expression and acceptor (PD-L1 or CD80) expression. In untreated cells, a lifetime decrease of 1.39±0.11ns to 1.19±0.12ns was detected, resulting in a FRET efficiency of 14.38% (Figure 1A). FRET Efficiency is correlated to molecular distance, Supplementary Table 1 indicates the range of receptor-ligand distances obtained for the following results. In cells treated with 25µg/ml of experimental blocking antibody J1201, the lifetime reduced from 1.35±0.10ns to 1.29±0.13ns, yielding a FRET efficiency of 4.44% (Figure 1B). iFRET signal was not observed when either primary staining antibody was omitted. Moreover, when each cell type was analysed alone, no interaction state was detected. The findings indicate that the decrease in donor lifetime reflected by the high FRET efficiency was due to the specific interaction of PD-1 and PD-L1, which was attenuated in the presence of J1201. In both cases intensity maps confirm the presence of the donor, PD-1 and acceptor, PD-L1. In Figure 1C, a Box and Whisker plot compares FRET efficiency values in the

absence and presence of experimental blocking antibody J1201 (25µg/ml). Each point on the graph represents one region of interest which may contain between 5 and 25 cells. Mean FRET efficiencies ± SEM are indicated. Mann Whitney U analysis determined statistical differences between treated and untreated cells (**, p=0.004).

Intercellular CTLA-4 and CD80 interactions, in Jurkat and Raji cells, were also assessed using iFRET (Figure 2). Here, in the absence of the blocking antibody ipilimumab, donor lifetime decrease from 1.96±0.17ns to 1.45±0.11ns in the presence of the acceptor. This resulted in a FRET efficiency of 26.02% (Figure 2A). When ipilimumab was added at 100µg/ml, the donor lifetime decreased from 2.06±0.12ns to 1.98±0.09ns, resulting in a FRET efficiency of 3.88% (Figure 2B). Intensity maps confirm the expression of CTLA-4 (donor) and CD-80 (acceptor). Box and Whisker plot (Figure 2C) compares FRET efficiency values in the absence and presence of 100µg/ml ipilimumab. Each point on the graph represents one region of interest which may contain between 5 and 25 cells. Mann-Whitney U analysis determined statistical differences between treated and untreated cells (***, $p=3.27x10^{-7}$).

To benchmark the effectiveness of the iFRET assay in clinically relevant settings, we compared the assay to a Proximity Ligation Assay (PLA), which in principle can also visualise PD-1 and PD-L1 within proximities of approximately 40nm. To achieve this comparison, iFRET and PLA analyses were run on sequential ccRCC tissue sections from the same tissue block. Prior to the investigation, samples were determined PD-L1 positive (>1%) or negative (<1%) using the Roche VENTANA PD-L1 (SP142) assay.

PLA allowed the qualitative visualisation of PD-1 and PD-L1 within close proximity (Supplementary Figure 3A). The PD-L1 positive ccRCC sample labelled with anti-PD-1, anti-PD-L1 and PLA +/- probes produced measurable PLA signals, albeit comparatively weak signals. Furthermore, PLA signals were observed across both experimental and control groups (normal renal tissue) possibly due to PLA only determining close proximity (up to 40nm) as opposed to direct interaction (≤10nm) limiting the specificity of the assay (24).

The Box and Whisker plots show the interaction states in the PD-L1 positive and PD-L1 negative groups. In the PD-L1 negative group, PLA fails to detect an interaction whereas iFRET detects two areas of significant interaction (Supplementary Figure 3B). These observations suggest that iFRET provides greater sensitivity and specificity than PLA, allowing the identification of tumour-mediated immune-suppression in patients otherwise considered as PD-L1 negative.

PD-L1 expression does not correspond to interaction status of PD-1 and PD-L1 in ccRCC

Following iFRET optimisation and benchmarking, we assessed the interaction of PD-1 and PD-L1 in the subsequent FFPE ccRCC tissue sections from the above cohort of patients with as yet unknown outcomes. The series included samples from 22 patients considered as PD-L1 negative (<1%) or positive (>1%), as determined using the Roche VENTANA PD-L1 (SP142) assay and multi-site tumour sampling (MSTS). Three regions of interest per patient sample were analysed and the mean FRET efficiency for each patient calculated. Across these patients, mean FRET

efficiencies varied from 0.17% to 14.1%, indicating iFRET is able to quantitatively detect the heterogeneity of PD-1 and PD-L1 interaction states in patients. Figure 3A shows a sample with a donor lifetime decrease of 1.91±0.18ns to 1.58±0.19ns this results in a FRET efficiency of 17.28%. Notably, PD-L1 expression, classified by MSTS, did not correlate with the interaction status of PD-1 and PD-L1 as determined by iFRET (Figure 3B). Crucially, iFRET detected significant interaction states in 11 out of the 12 PD-L1 negative patients, a functional state that was not detected by conventional IHC methods. Conversely, one PD-L1 positive patient showed a minimal interaction state (Figure 3B).

PD-1/PD-L1 interaction state is indicative of patient outcome in malignant melanoma

After analysing PD-1/PD-L1 interaction in ccRCC tissue, the interaction status in 176 malignant melanoma patients with known outcomes was assessed. The cohort, which consisted of treated and untreated patients, was predominantly male with a split of 102M/71F and a mean age of 66.1 years. 25% of patients had stage I tumours, 43.5 had stage II tumours, 9.4% had stage III tumours and 22.1% had stage IV tumours. Tumour infiltrating lymphocytes were absent in 39 patients, 101 patients had focal infiltration with 30 patients experiencing extensive infiltration (Supplementary Table 2). Of the 176 patients, 148 were untreated, 14 received immunotherapies (nivolumab, pembrolizumab or ipilimumab) and 14 received non-immune therapies (radiotherapy, chemotherapy or small molecule inhibitors (Vemurafenib, Trametinib, Dabrafenib)).

Figure 4A shows the Haematoxylin and Eosin (H&E) staining of a primary cutaneous malignant melanoma. The left-hand panels show the H&E staining of patient 390, a non-ulcerated tumour sample with no tumour infiltrating lymphocytes, this patient had a FRET efficiency of 3.50%. The top panel shows a 5X magnification with the lack of ulceration circled, subsequent 10X magnifications show the lack of tumour infiltrating lymphocytes. The right-hand panels show patient 131, with high tumour infiltrating lymphocytes, this patient had a FRET efficiency 26.20%. The top panel here shows a 5X magnification indicating the tumour infiltrating lymphocytes (black circled area) and tumour ulceration (blue circle). The subsequent middle and bottom panels show 10X magnifications of lymphocyte infiltration and tumour ulceration respectively. Figure 4B shows FLIM images of the sample of patient 390, where intensity maps illustrate the expression of PD-1 and PD-L1. Here, the pseudo-colour scale runs from 3.5ns (blue) to 0.5ns (red). Despite a high expression of PD-L1 in this patient's sample, a low change in donor lifetime was observed; donor lifetime alone was 1.95±0.16ns and slightly decreased to 1.88±0.15ns in the presence of the acceptor. The resulting FRET efficiency is 3.50%. Conversely, Figure 4C shows the sample of patient 131. As observed in the sample of patient 390, patient 131s' sample demonstrated a prominent level of PD-L1 expression. However, unlike patient 390, patient 131 displayed a high interaction state between ligand and receptor, with the donor lifetime decreasing from 2.22±0.19ns to 1.64±0.15ns when in the presence of the acceptor, with a resulting FRET efficiency of 26.20%.These results reinforce the hypothesis that PD-L1 expression does not correlate with PD-1/PD-L1 interaction.

The interaction state was assessed with respect to clinical PD-L1 expression scores for 159 of the 176 patients in this cohort (PD-L1 scores were not available for the remaining 17 patients). Figure 5A shows the lack of correlation between clinical PD-L1 expression scores and interaction state determined by iFRET. Here, the clinical IHC images of patient 390 (bottom) and patient 131 (top) are shown. As this was performed on a TMA, each patient had one FRET efficiency value, with each point of the Box and Whisker plot representing one patients FRET efficiency. Out of the 117 patients who were stratified as being PD-L1 negative, 58 showed a PD-1/PD-L1 interaction state; a functional state not detected by conventional IHC methods. Of the 42 patients who were in the PD-L1 positive group, 19 showed no interaction despite the presence of the ligand.

We then correlated PD-1/PD-L1 interaction state with patient survival. The cohort were ranked in order of their FRET efficiency values and sorted into the following categories; those with the lowest 80% of FRET efficiencies and those with the highest 20%. In Figure 5B, Kaplan-Meier survival analysis revealed that those with the lowest 80% of FRET efficiencies had a significantly worse outcome than those with the highest 20% (Log-Rank (Mantel-Cox) $p=0.05$). Cox-Regression for Survival Analysis revealed PD-1/PD-L1 interaction was the only significant factor impacting overall survival ($p=0.019$). We then sought to apply Kaplan-Meier analysis to correlate the clinical PD-L1 scores with patient outcome. In Figure 5C, there is no significant difference in outcome between the PD-L1 positive and PD-L1 negative patients (Log-Rank (Mantel-Cox) $p=0.87$). This illustrates that iFRET is more informative on patient outcome than conventional IHC approaches reporting ligand

expression.

Lower PD-1/PD-L1 interaction states correlate with worsened overall and progression-free survival in metastatic NSCLC.

Next, in an outcome blinded study, we applied iFRET to samples from patients with metastatic NSCLC. A statistical power calculation indicated that, to obtain results with at least 80% significance, a sample number of >30 was required, hence we tested 60 FFPE samples, all from anti-PD-1 post-treatment patients. Of these 60 patients, 40 had clinical follow-up and outcome and were used to create Kaplan-Meier survival plots. The cohort comprised of 36 males and 24 females with an age range of 44-86 years (median ages 63 years) (Supplementary Table 3). Performance status was defined, and 50 patients had a performance status of ≤1 and 10 patients had a status of ≥1 (see methods).

Pathologist assessment highlighted regions of interest within each sample by identifying tumours and regions of immune-cell infiltration for each sample. In order to analyse the whole region of interest within a patient sample, multiple sub-regions were analysed for PD-1/PD-L1 interaction state, resulting in a range of FRET efficiencies for each patient. Figure 6A shows FLIM images demonstrating that as in other tumour settings (see above) PD-1 and PD-L1 expression levels do not correlate with interaction state. The pseudo-colour scale (ranging from 1.0ns to 2.7ns) illustrates a donor lifetime decrease from 1.99±0.17ns to 1.44±0.14ns yielding a FRET efficiency of 27.64%. Figure 6B is a Box and Whisker plot where each plot represents one patient. Each plot represents all the FRET efficiency values obtained for each patient, with the median value

written above each plot. The highest median FRET efficiency value was 29.90% with the lowest being 0.00%. The Box and Whisker diagram demonstrates the ability of iFRET to quantify inter- and intra-patient heterogeneity of PD-1/PD-L1 interactions in metastatic NSCLC (Figure 6B).

The survival data of 40 patients was subsequently analysed and correlated to each patient's FRET efficiency, indicating their PD-1/PD-L1 interaction state. Patients were then ranked in order of their median FRET efficiency and split into the following two groups; those with the highest 40% of median FRET efficiencies and those with the lowest 60% of median FRET efficiencies. Kaplan-Meier survival analysis demonstrated that for these anti-PD-1 treated patients, those with the lowest 60% median FRET efficiency values, and therefore a lower PD-1/PD-L1 interaction state had a significant worsened overall survival ($p=0.05$) (Figure 7A). When analysing PD-L1 expression (indicated by acceptor intensity) Kaplan-Meier analysis failed to determine a difference between those with a high PD-L1 expression and those with a low PD-L1 expression ($p=0.97$) (Figure 7B). This again shows the shortcomings of using PD-L1 expression levels to determine patient outcome.

Discussion

This study has demonstrated the application of iFRET to detect intercellular ligand-receptor interactions. The method combines a two-site time-resolved FRET assay and signal amplification, with a tissue preparation time identical to that of IHC approaches. The high-throughput frequency domain FRET/FLIM imaging platform allowed mapping and automated acquisition of data from both cell cultures and arrayed tissue samples, thereby creating a straightforward procedure for non-specialised personnel (Supplementary Methods). The automatic detection of regions of interest within the acquisition process significantly reduced operator bias.

This assay measures receptor-ligand distances of 1-10nm and determines interaction as any distance that falls within this range. Currently, alternative assays have utilised PD-1 and PD-L1 expression to determine receptor-ligand proximity. Tumeh et al., 2014 have applied an assay which determines the presence of PD-1 and PD-L1 in close proximity to be an interaction (25). However, the working distances of intensity colocalization assays are far greater (70nm-20μm) than that of iFRET. Moreover, when expression readouts have been used in the pathologies assessed here, PD-L1 expression has not correlated with interaction state or patient outcome.

The iFRET methodology was exemplified for assessing the interaction status of two immune-checkpoint pairs, PD-1/ PD-L1 and CTLA-4/CD80, in single-cell assays and biopsy tissue samples from patients with ccRCC, primary malignant melanoma and metastatic NSCLC. The initial validation of the method in single-cell co-culture assays, where manipulation of ligand-receptor interactions can be specifically suppressed, has provided the confidence to assess these complexes in patient biopsies. The additional controls with respect to the use of single antibodies and single secondary reagents add further to the validity of the assay platform and of course are controls than can be applied routinely to patient biopsies.

Comparison of iFRET with PLA provided evidence that the latter did not perform as well in these settings in identifying interaction. By its very design, the iFRET methodology elaborated here provides both a measure of ligand-receptor interaction and the spatial resolution of this interaction. Importantly this is readily achieved in routinely fixed

samples from patient biopsies, offering great promise in being able to inform on the more detailed behaviour of these interactions and their distribution within pathological settings. This is well illustrated here with the observed heterogeneity seen not simply between patient biopsies but within individual biopsies reflected in the spread of FRET efficiencies across regions of interest for individual patients. This heterogeneity may reflect differential patterns of reprogramming of the tumour microenvironment playing out in modified immune-suppressive ligand presentation and/or variability in the degree of immune-cell infiltration.

A lack of correlation between the extent of PD-1/PD-L1 interaction state and the expression levels of these two proteins was evident in ccRCC, malignant melanoma and metastatic NSCLC cohorts. In both melanoma and NSCLC, it was shown that PD-L1 expression levels were unable to predict patient outcome. This questions current protocols which rely on IHC PD-L1 expression levels to predict patient outcome and thus has implications for the use of simple expression levels to stratify patients for treatment. Moreover, in ccRCC patients, high interaction states were observed in patients who would otherwise be labelled as PD-L1 negative. Blockade of interaction would be predicted to be effective in contexts where elevated levels of interaction occurs and is by inference responsible for the immune privileged state of the tumour. Hence interaction would *a priori* be a criterion for treatment.

To examine the potential impact of this approach further, a unique cohort of patients with metastatic NSCLC were studied. The cohort of patients from which the FFPE samples were derived, were all

treated with anti-PD-1 monotherapies and had full clinical follow-up and outcomes. Within this cohort, iFRET has shown the potential for a high versus low PD-1/PD-L1 interaction state to be utilised as a predictive clinical biomarker post-treatment. Conceptually it is surmised that a high degree of PD-1/PD-L1 interaction infers tumour selection in patients, indicating that the patient's tumour may be reliant on PD-1/PD-L1 interaction to facilitate immune evasion. It is precisely this group of patients that would be expected to respond to immune checkpoint inhibition.

As these were post-treatment samples from responsive patients with metastatic NSCLC, it was questioned why a high level of PD-1/PD-L1 interaction state might be observed? The pharmacodynamics of immune-checkpoint disruption as a measure of target interaction has not been monitored to date. As such it is not known whether blockade of checkpoint interaction needs to be either sustained or complete. The working hypothesis derived from this dataset is that interaction is likely incomplete and as such, that a threshold level of T lymphocyte complex disengagement is sufficient to trigger the observed responses to intervention. It will be informative in a suitable setting to monitor complex disengagement as a function of time following treatment.

Those patients with low interaction and therefore worsened survival may nevertheless benefit from alternative immune therapies. These tumours may evade the immune system by dysregulating CTLA-4/CD-80 or other inhibitory interactions. Furthermore, no tumour will discretely dysregulate one pathway, in fact, a tumour may evolve to evade host immune response by modulating multiple pathways

simultaneously, indicating a patient group who would benefit from dual checkpoint inhibitor therapies (26,27).

iFRET can be exploited to monitor other intercellular protein interactions and there are ongoing developments designed to capture related immune modulatory interactions pertinent to cancer and emerging cancer treatments. This provides the potential for iFRET to become a useful predictive tool informing on the nature of the tumour immune-privileged state. However, as a principle, it is clear that this approach has capabilities beyond immune-tumour cell interactions and the broader uptake of the approach promises to be informative in many research (e.g. axon guidance) and clinical (e.g. angiopathies) settings.

The exemplification of iFRET in tumour settings opens up exciting and powerful new opportunities to move beyond the cataloguing of cell phenotypes *in situ* and add functional attributes to our patient data inventory, impacting clinical decisions. This is a routine parameter for small molecule inhibitors targeted at driver mutations and we suggest it should become a routine for these more complex biotherapeutic interventions.

Acknowledgments

This work was supported in part by Department of Education, Basque Government- IT1270-19, Elkartek Grant (BG18) and the Spanish Ministry Grant (MINECO) PROJECTS of EXCELLENCE (BFU2015-65625-P). Peter J Parker is supported by a core grant to the Francis Crick Institute, from Cancer Research UK (CRUK) (FC001130), the UK Medical Research Council (MRC) (FC001130), and the Wellcome Trust (FC001130). We would like to thank Pierre Leboucher for the automation of the multiple frequency domain FLIM and Patel Poulam, Clinical Oncologist at Nottingham, for clinical discussions. We would also like to thank Audrey Colomba at the Francis Crick Institute for her help in PLA image acquisition.

References

1. Douglas Hanahan RW. Biological Hallmarks of Cancer. Holland-Frei Cancer Medicine2017. p 1-10.
2. Pardoll DM. The blockade of immune checkpoints in cancer immunotherapy. Nat Rev Cancer **2012**;12:252-64
3. Alsaab HO, Sau S, Alzhrani R, Tatiparti K, Bhise K, Kashaw SK*, et al.* PD-1 and PD-L1 Checkpoint Signaling Inhibition for Cancer Immunotherapy: Mechanism, Combinations, and Clinical Outcome. Front Pharmacol **2017**;8:561
4. Engelhardt JJ, Sullivan TJ, Allison JP. CTLA-4 Overexpression Inhibits T Cell Responses through a CD28-B7-Dependent Mechanism. The Journal of Immunology **2006**;177:1052-61
5. Okazaki T, Honjo T. The PD-1-PD-L pathway in immunological tolerance. Trends Immunol **2006**;27:195-201
6. Mahmoudi M, Farokhzad OC. Cancer immunotherapy: Wound-bound checkpoint blockade. Nature Biomedical Engineering **2017**;1:0031

7. Ross K, Jones RJ. Immune checkpoint inhibitors in renal cell carcinoma. Clin Sci (Lond) **2017**;131:2627-42
8. Heidegger I, Pircher A, Pichler R. Targeting the Tumor Microenvironment in Renal Cell Cancer Biology and Therapy. Front Oncol **2019**;9:490
9. Qin S, Xu L, Yi M, Yu S, Wu K, Luo S. Novel immune checkpoint targets: moving beyond PD-1 and CTLA-4. Mol Cancer **2019**;18:155
10. Sommer U, Eckstein M, Ammann J, Braunschweig T, Macher-Goppinger S, Schwamborn K*, et al.* Multicentric Analytical and Inter-observer Comparability of Four Clinically Developed Programmed Death-ligand 1 Immunohistochemistry Assays in Advanced Clear-cell Renal Cell Carcinoma. Clin Genitourin Cancer **2020**
11. Theelen W, Baas P. Pembrolizumab monotherapy for PD-L1 >/=50% non-small cell lung cancer, undisputed first choice? Ann Transl Med **2019**;7:S140
12. Roach C, Zhang N, Corigliano E, Jansson M, Toland G, Ponto G*, et al.* Development of a Companion Diagnostic PD-L1 Immunohistochemistry Assay for Pembrolizumab Therapy in Non-Small-cell Lung Cancer. Appl Immunohistochem Mol Morphol **2016**;24:392-7
13. Nunes-Xavier CE, Angulo JC, Pulido R, López JI. A Critical Insight into the Clinical Translation of PD-1/PD-L1 Blockade Therapy in Clear Cell Renal Cell Carcinoma. Current Urology Reports **2019**;20:1
14. Giraldo NA, Nguyen P, Engle EL, Kaunitz GJ, Cottrell TR, Berry S*, et al.* Multidimensional, quantitative assessment of PD-1/PD-L1 expression in patients with Merkel cell carcinoma and association with response to pembrolizumab. J Immunother Cancer **2018**;6:99
15. Johnson DB, Bordeaux J, Kim JY, Vaupel C, Rimm DL, Ho TH*, et al.* Quantitative Spatial Profiling of PD-1/PD-L1 Interaction and HLA-DR/IDO-1 Predicts Improved Outcomes of Anti-PD-1 Therapies in Metastatic Melanoma. Clin Cancer Res **2018**;24:5250-60
16. Delahunt B, Cheville JC, Martignoni G, Humphrey PA, Magi-Galluzzi C, McKenney J*, et al.* The International Society of Urological Pathology (ISUP) grading system for renal cell carcinoma and other prognostic parameters. Am J Surg Pathol **2013**;37:1490-504

17. Lopez JI, Cortes JM. Multisite tumor sampling: a new tumor selection method to enhance intratumor heterogeneity detection. Hum Pathol **2017**;64:1-6
18. Oken MM, Creech RH, Tormey DC, Horton J, Davis TE, McFadden ET*, et al.* Toxicity and response criteria of the Eastern Cooperative Oncology Group. Am J Clin Oncol **1982**;5:649-55
19. Veeriah S, Leboucher P, de Naurois J, Jethwa N, Nye E, Bunting T*, et al.* High-throughput time-resolved FRET reveals Akt/PKB activation as a poor prognostic marker in breast cancer. Cancer Res **2014**;74:4983-95
20. Miles J, Applebee CJ, Leboucher P, Lopez-Fernandez S, Lee DJ, Guarch R*, et al.* Time resolved amplified FRET identifies protein kinase B activation state as a marker for poor prognosis in clear cell renal cell carcinoma. BBA Clin **2017**;8:97-102
21. Lausen B, Schumacher M. Maximally Selected Rank Statistics. Biometrics **1992**;48:73-85
22. Hothorn T, Lausen B. On the exact distribution of maximally selected rank statistics. Comput Stat Data Anal **2003**;43:121–37
23. Söderberg O, Leuchowius KJ, Gullberg M, Jarvius M, Weibrecht I, Larsson LG*, et al.* Characterizing proteins and their interactions in cells and tissues using the in situ proximity ligation assay. Methods **2008**;45:227-32
24. Debaize L, Jakobczyk H, Rio AG, Gandemer V, Troadec MB. Optimization of proximity ligation assay (PLA) for detection of protein interactions and fusion proteins in non-adherent cells: application to pre-B lymphocytes. Mol Cytogenet **2017**;10:27
25. Tumeh PC, Harview CL, Yearley JH, Shintaku IP, Taylor EJ, Robert L*, et al.* PD-1 blockade induces responses by inhibiting adaptive immune resistance. Nature **2014**;515:568-71
26. Autio KA, Boni V, Humphrey RW, Naing A. Probody Therapeutics: An Emerging Class of Therapies Designed to Enhance On-target Effects with Reduced Off-tumor Toxicity for Use in Immuno-Oncology. Clinical Cancer Research **2019**:clincanres.1457.2019
27. Intlekofer AM, Thompson CB. At the bench: preclinical rationale for CTLA-4 and PD-1 blockade as cancer immunotherapy. J Leukoc Biol **2013**;94:25-39

Figure Legends:

Figure 1: iFRET detects and quantifies PD-1/PD-L1 interaction between CHO-K1 and Jurkat cells. A) FLIM images consist of greyscale expression maps indicating PD-1 expression (donor, ATTO488) and PD-L1 expression (acceptor, ALEXA594). Pseudo-colour lifetime maps indicate the lifetime of the donor alone and lifetime of the donor in the presence of the acceptor. A lifetime decrease of 1.39±011ns to 1.19±0.12ns yields a FRET efficiency of 14.38% in untreated cells. **B)** When treated with 25 µg/ml J1201 (experimental anti-PD1 blocking antibody) the donor lifetime decreased from 1.35±0.10ns to 1.29±0.13ns. This gives a FRET

efficiency of 4.44%, indicating a significant reduction of PD-1/PD-L1 interaction. **C)** Box and Whisker plot compares FRET efficiency values in the absence and presence of experimental blocking antibody J1201 (25µg/ml). Each point on the graph represents one region of interest which may contain between 5 and 25 cells. Mean FRET efficiencies ± SEM are indicated. Mann Whitney U analysis determined statistical differences between treated and untreated cells (**, p=0.004).

Figure 2: iFRET precisely determines CTLA-4/CD-80 interaction between Raji and Jurkat cells. A) In untreated Raji and Jurkat cells, the donor lifetime decrease from 1.96±0.17ns alone to 1.45±0.11ns in the presence of the acceptor. This gives a FRET efficiency of 26.02%. **B)** When treated with 100µg ipilimumab, donor lifetime decreased from 2.06±0.12ns to 1.98±0.09ns. This results in a FRET efficiency of 3.88%. **C)** Box and Whisker plot compares FRET efficiency values in the absence and presence of 100µg/ml ipilimumab. Each point on the graph represents one region of interest which may contain between 5 and 25 cells. Mann-Whitney U analysis determined statistical differences between treated and untreated cells (***, $p=3.27x10^{-7}$).

Figure 3: iFRET detects heterogeneity of PD-1 and PD-L1 interaction in FFPE ccRCC. A) Intensity images and lifetime maps (pseudo-colour scale) of FFPE human ccRCC patient sample 16-15203. A decrease in donor lifetime from1.91±0.18ns alone, to 1.58±0.19ns in the presence of the acceptor gives a FRET efficiency of 17.28%. **B)** Box and Whisker plots shown the interaction state of each patient in either the PD-L1 negative or PD-1 positive group.

Here, iFRET identifies that 11 of the 12 PD-L1 negative patients had a significant interaction state. Conversely, 1 patient in the PD-L1 positive group exhibited no interaction state.

Figure 4: PD-L1 expression does not correlate with PD-1/PD-L1 interaction state in malignant melanoma. A) The left-hand panels show the H&E staining of the sample of patient 390 with a FRET efficiency of 3.50%. The top panel shows a scanning view of the non-ulcerated (blue circle) tumour at 5X with the subsequent images showing high power (10X) images of the tumour, highlighting a lack of tumour infiltrating leukocytes. Right hand panels show the H&E staining of patient 131 with a FRET efficiency of 26.20%. The top panel shows a scanning view of the tumour with the tumour infiltrating leukocytes shown (black marked area) and tumour ulceration (blue circle). The middle and bottom panels show tumour leukocyte infiltration and tumour ulceration respectively at a magnification of 10X. **B)** Fluorescence lifetime imaging microscopy (FLIM) images show a melanoma with a low PD-1/PD-L1 interaction state. Expression images, based on PD-1 or PD-L1 intensity, show the presence of the receptor and ligand, however, the lifetime map shows no change in pseudo-colour, indicating a lifetime change of 1.95±0.16ns to 1.88±0.15ns and thus no interaction state **C)** FLIM images show a melanoma sample with a high PD-1/PD-L1 interaction state. Again, the expression maps show the presence of PD-1 and PD-L1 as in panel B, however the change in pseudo-colour represents a change in lifetime of 2.22±0.19ns to 1.64±0.15, indicating a high interaction state.

Figure 5: PD-1/PD-L1 interaction state predicts patient outcome

in malignant melanoma where PD-L1 expression fails to do so. A) PD-L1 was labelled and patients clinical PD-L1 expressions were determined as PD-L1 negative or PD-L1 positive. PD-L1 expression status was correlated with interaction state. Within the patients' assessed as PD-L1 negative, iFRET determined 58 patients which show an interaction state, with 59 patients in the PD-L1 negative group showing no interaction state. Conversely, in those patients clinically stratified as PD-L1 positive, iFRET determines that 19 out of 42 patients show no interaction state. The IHC PD-L1 images of patients 390 and 131, with FRET efficiencies of 3.50% and 26.2% respectively are shown. **B)** Kaplan-Meier survival analyses comparing patients with the highest 20% of FRET efficiencies and those with the lowest 80% (n=176). Those with a lower PD-1/PD-L1 interaction state (lower FRET efficiency) had an improved overall survival compared to those with a higher interaction state (Log Rank (Mantel-Cox) p=0.05), underpinning the ability of iFRET to predict patient outcome. **C)** Clinical PD-L1 scores defined patients as being PD-L1 positive or PD-L1 negative. Kaplan-Meier analysis detected no significant difference in patient outcome when correlated with PD-L1 expression (Log Rank (Mantel-Cox) p=0.87) exhibiting that PD-L1 expression levels fail to predict patient outcome

Figure 6: iFRET quantifies PD-1/PD-L1 interaction state in metastatic NSCLC alongside inter- and intra-patient heterogeneity. A) FLIM images show intensity and lifetime maps of a FFPE metastatic NSCLC sample. Intensity images show PD-1 and PD-L1 expressions respectively. The pseudo-colour scale illustrates a donor lifetime decrease from 1.99±0.17ns to 1.44±0.14ns yielding a FRET efficiency of 27.64%. B**)** Box and Whisker plots quantify the

interaction states observed with each plot representing the interaction states detected within each patient sample. Values above each plot represent the median FRET efficiency value for each patient sample. The highest median FRET efficiency value observed was 29.90% and the lowest 0.00%. iFRET not only quantifies inter-patient heterogeneity but also intra-patient heterogeneity.

Figure 7: Lower PD-1/PD-L1 interaction correlates to a significantly worsened patient survival in metastatic NSCLC. A) Anti-PD-1 post-treatment patients were ranked by their mean FRET efficiency value and grouped into the following: the lowest 60% of median FRET efficiencies and the highest 40% of median FRET efficiencies. Those with the lowest 60% of median FRET efficiencies had a significantly ($p=0.05$) worsened overall survival. **B)** Patients were ranked by their PD-L1 expression (acceptor intensity) and split into the lowest 60% of median acceptor intensities and the highest 40%. Kaplan-Meier survival analysis was unable to detect a difference between the two groups (Log Rank (Mantel-Cox) $p=0.97$).

Figure 1: Sanchez-Magraner, and Miles et al., 2020.

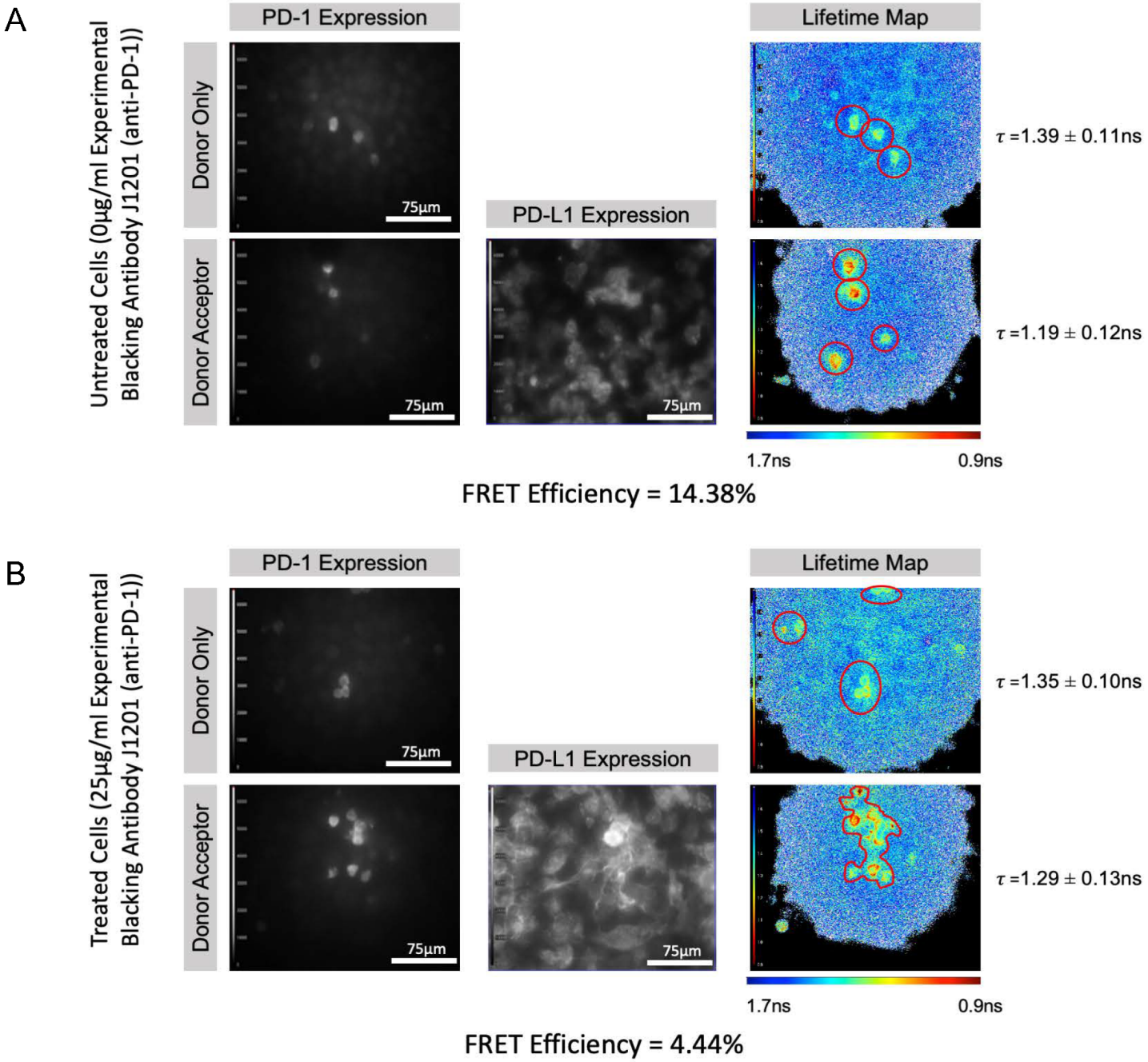

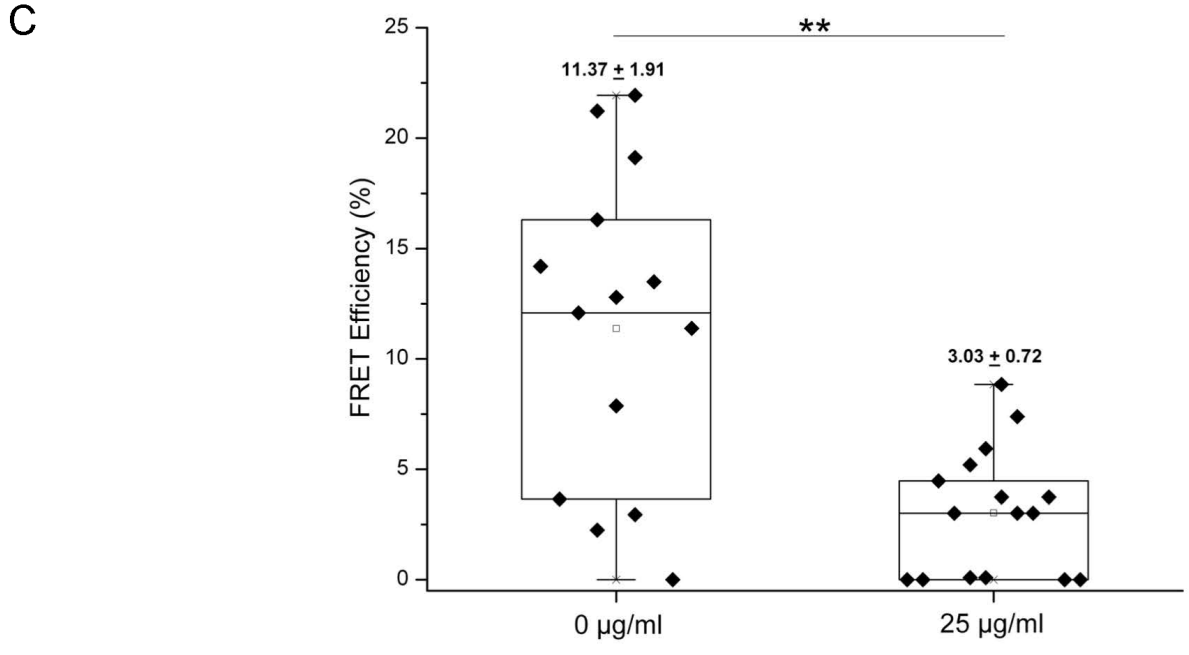

Figure 2: Sanchez-Magraner, and Miles et al., 2020.

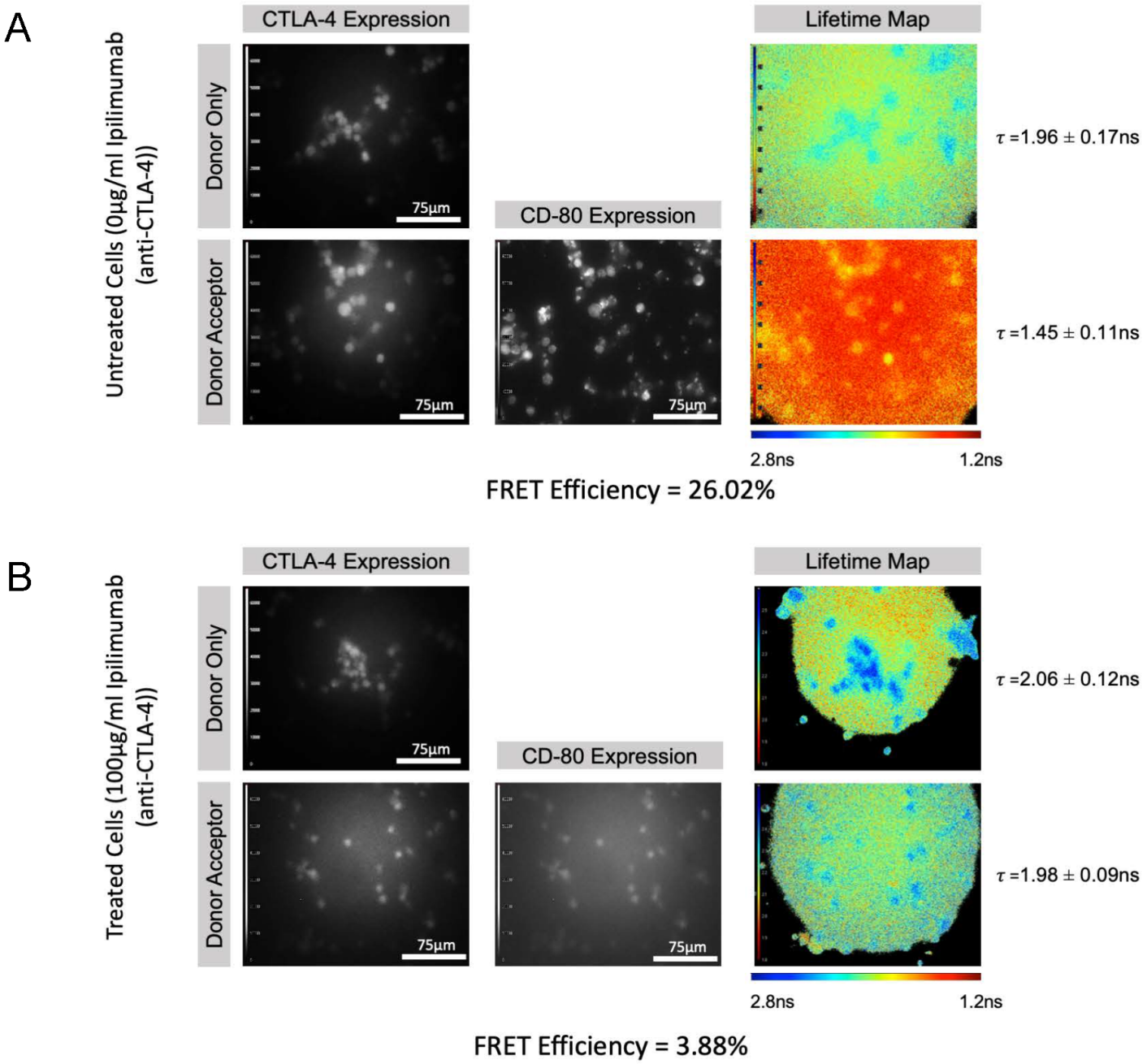

Figure 3: Sanchez-Magraner and Miles et al., 2020.

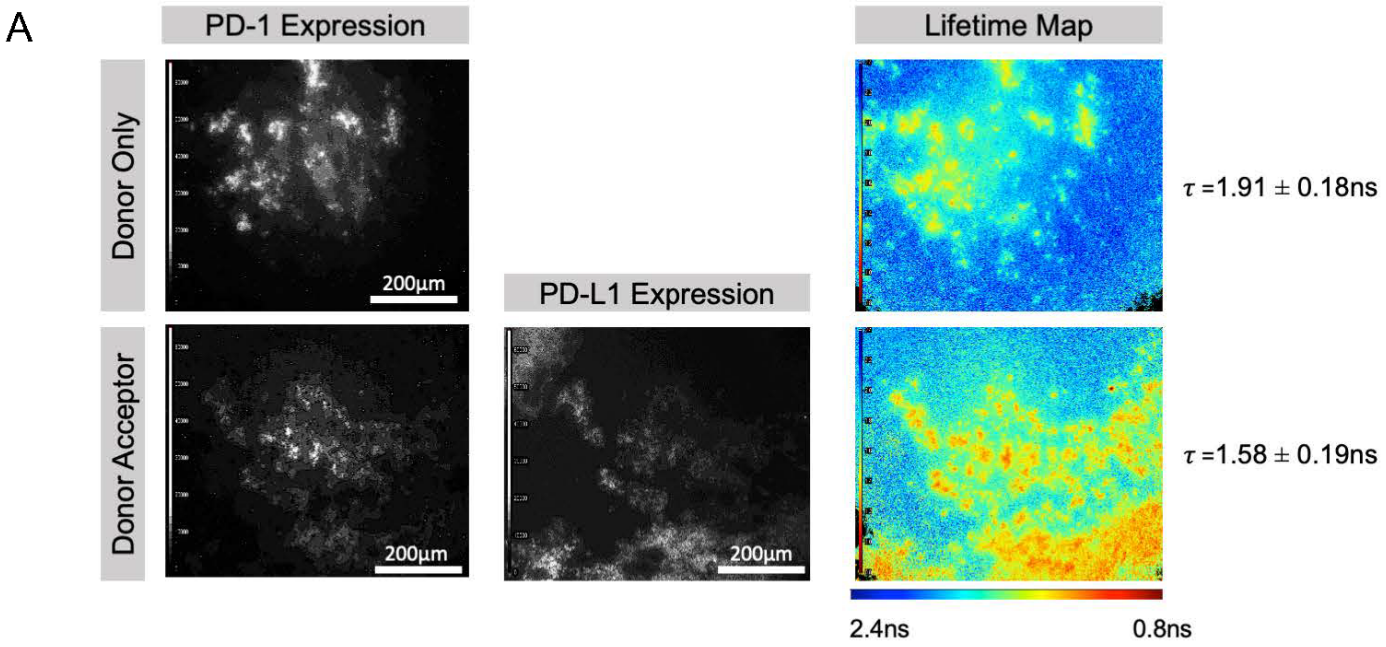

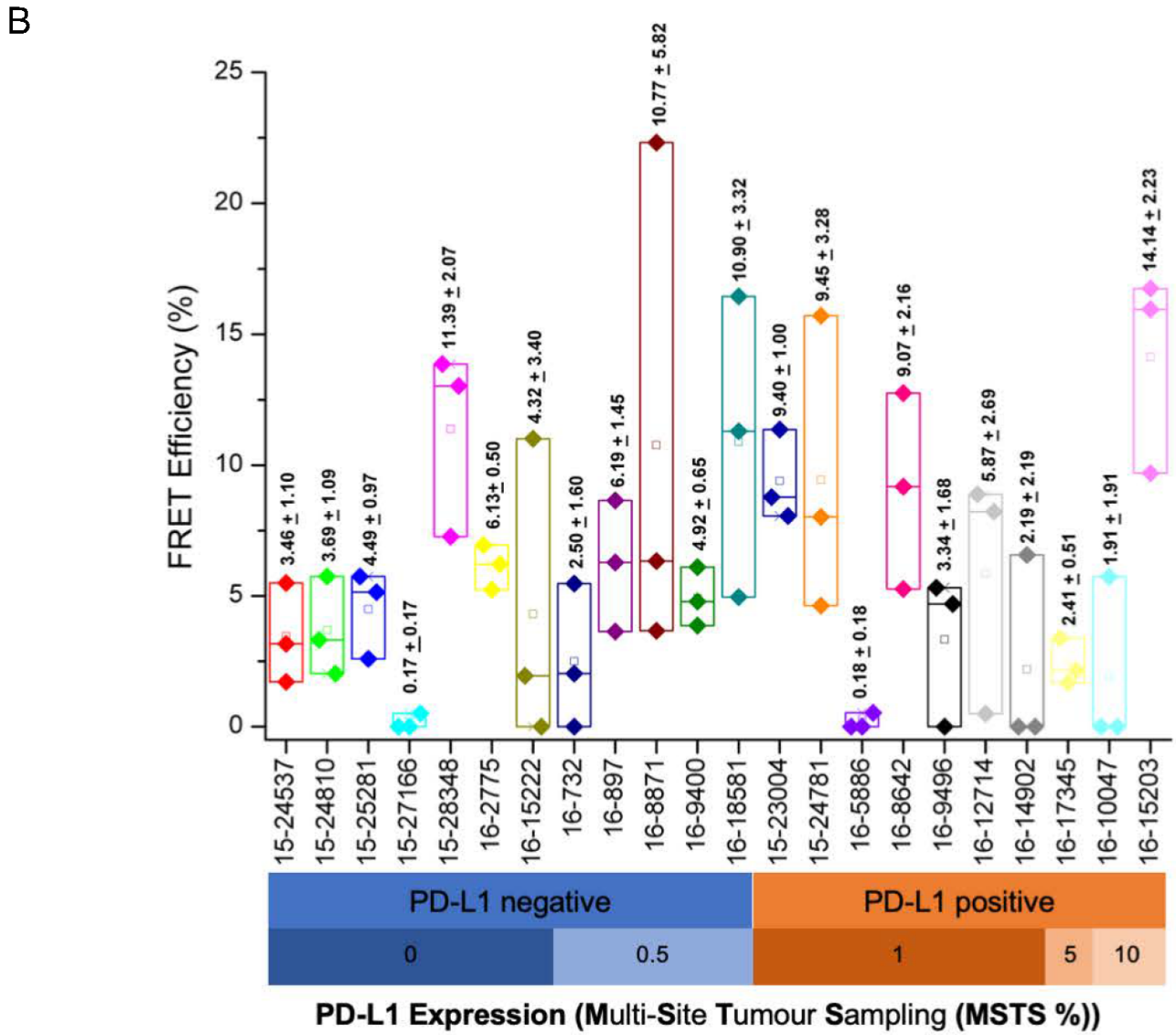

Figure 4: Sanchez-Magraner and Miles 2019.

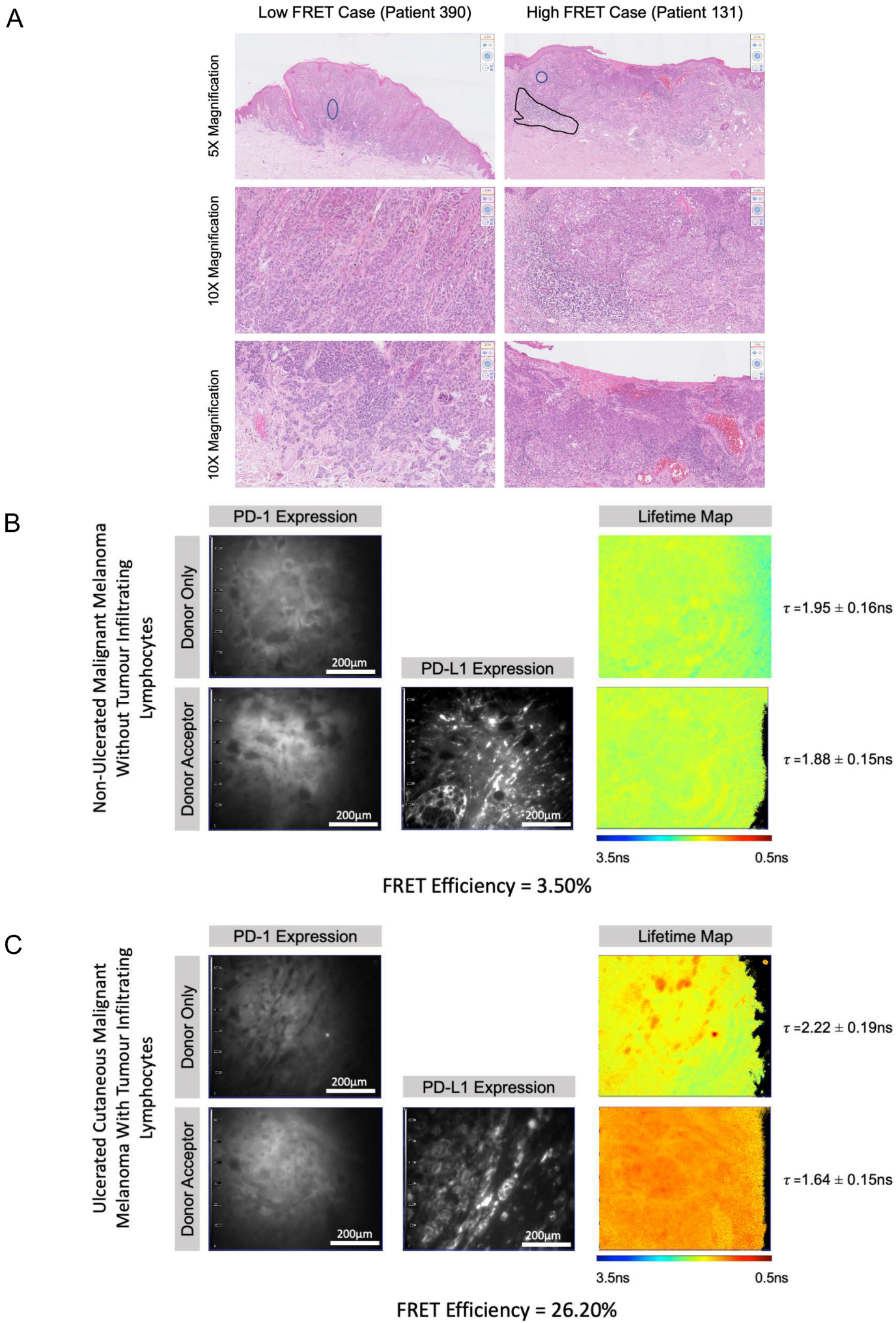

Figure 5: Sanchez-Magraner and Miles et al., 2020.

A

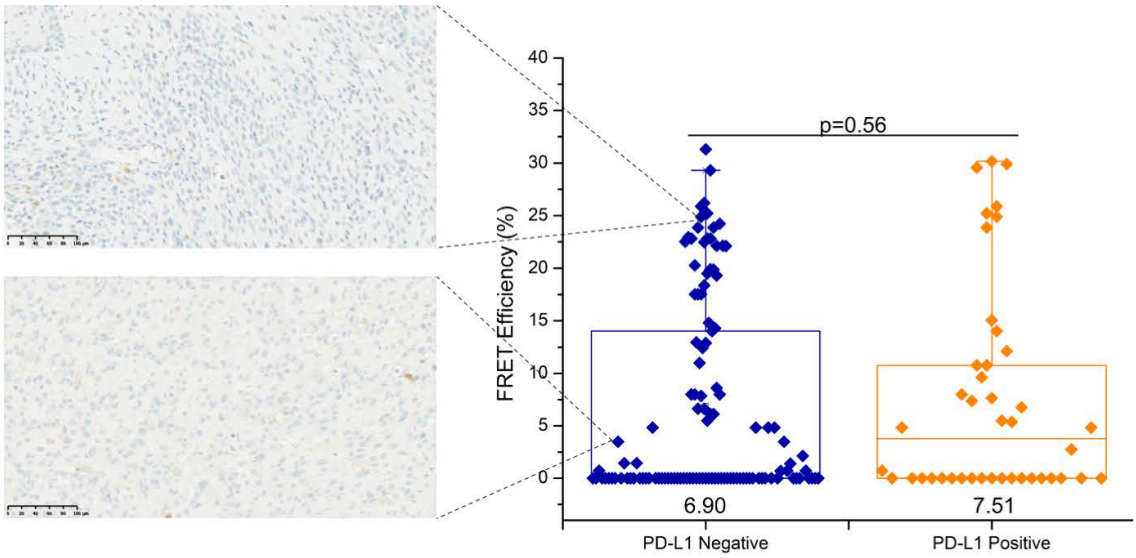

B

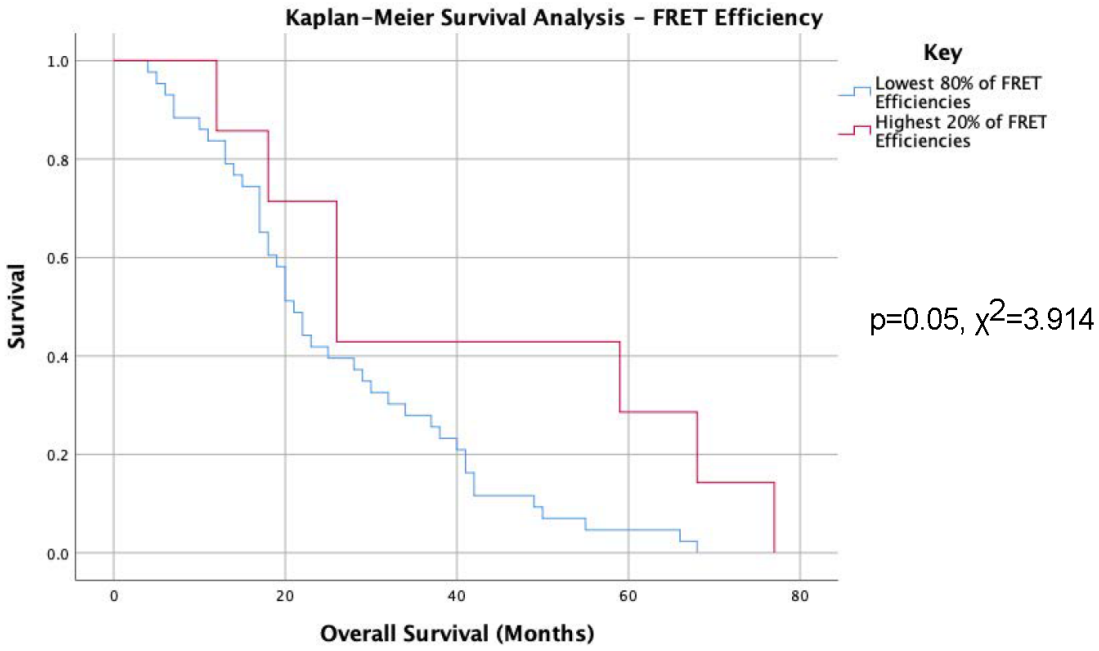

C

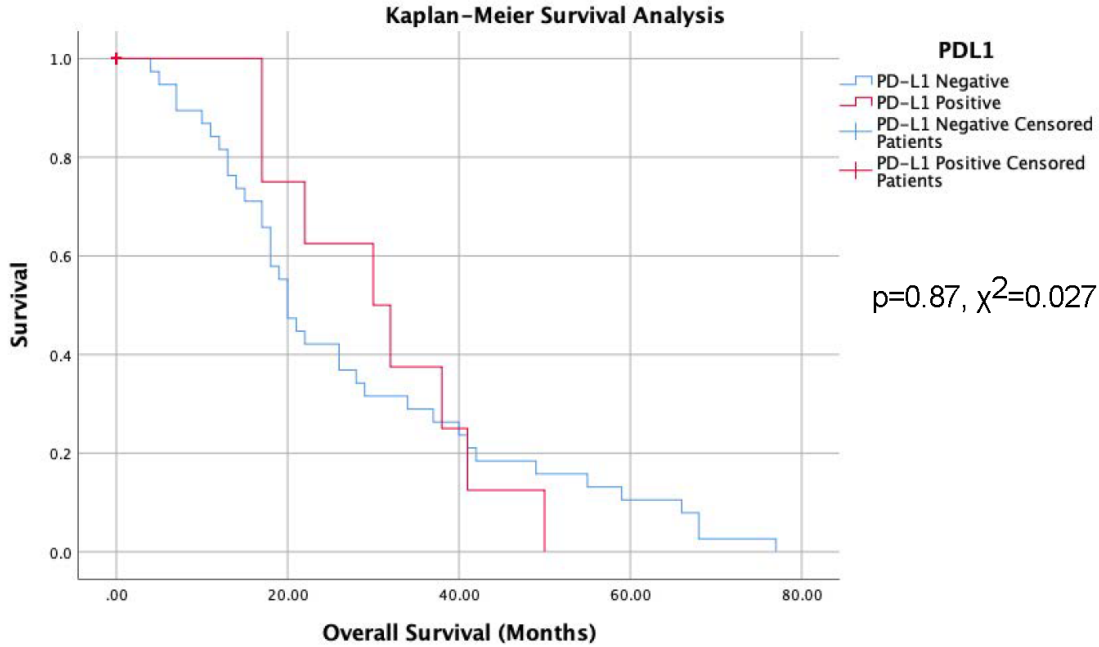

Figure 6: Sanchez-Magraner and Miles et al., 2020.

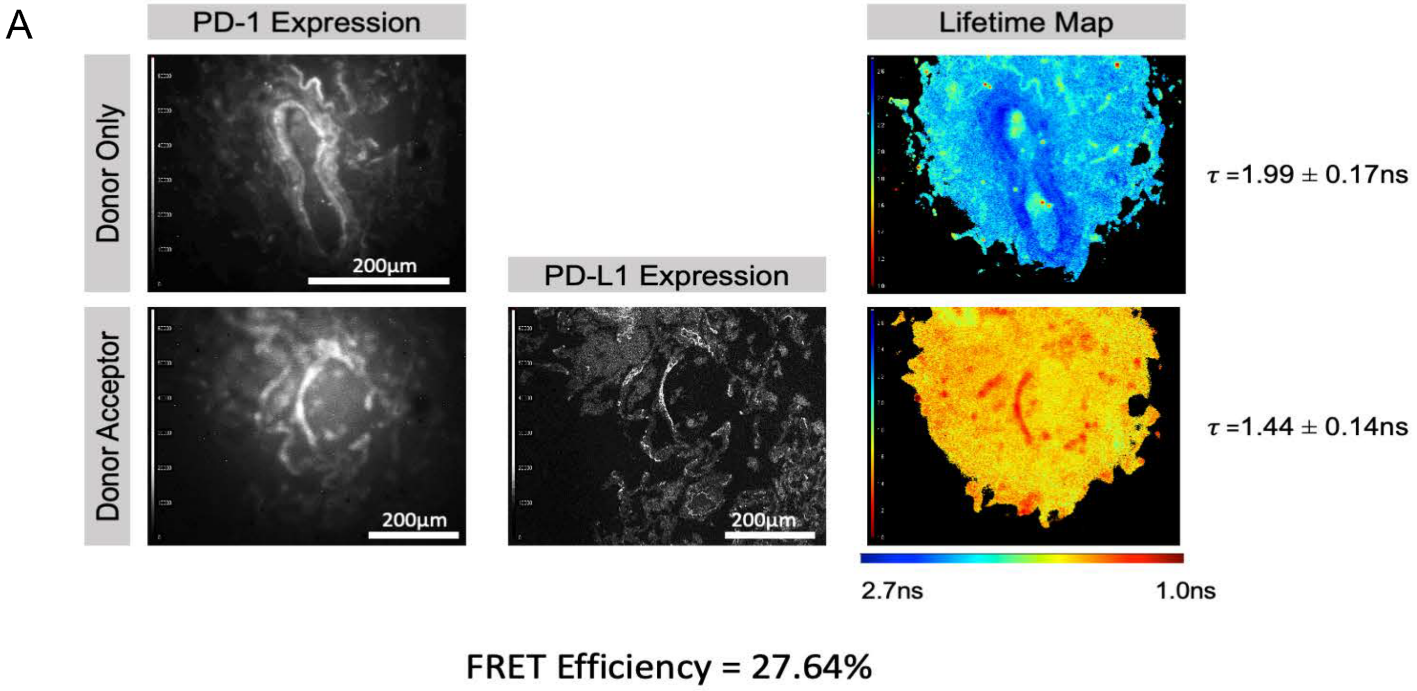

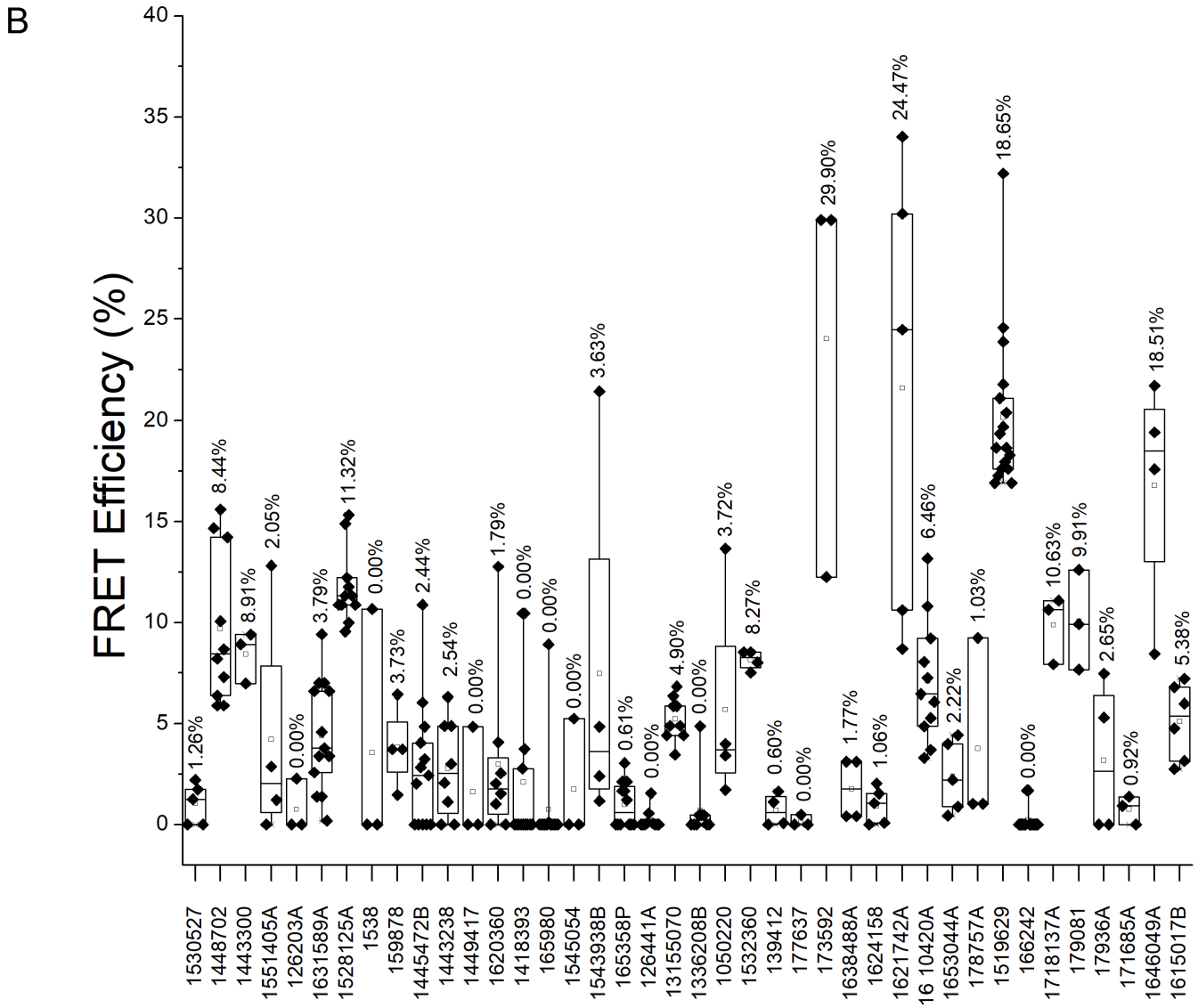

Figure 7: Sanchez-Magraner and Miles et al., 2020.

A

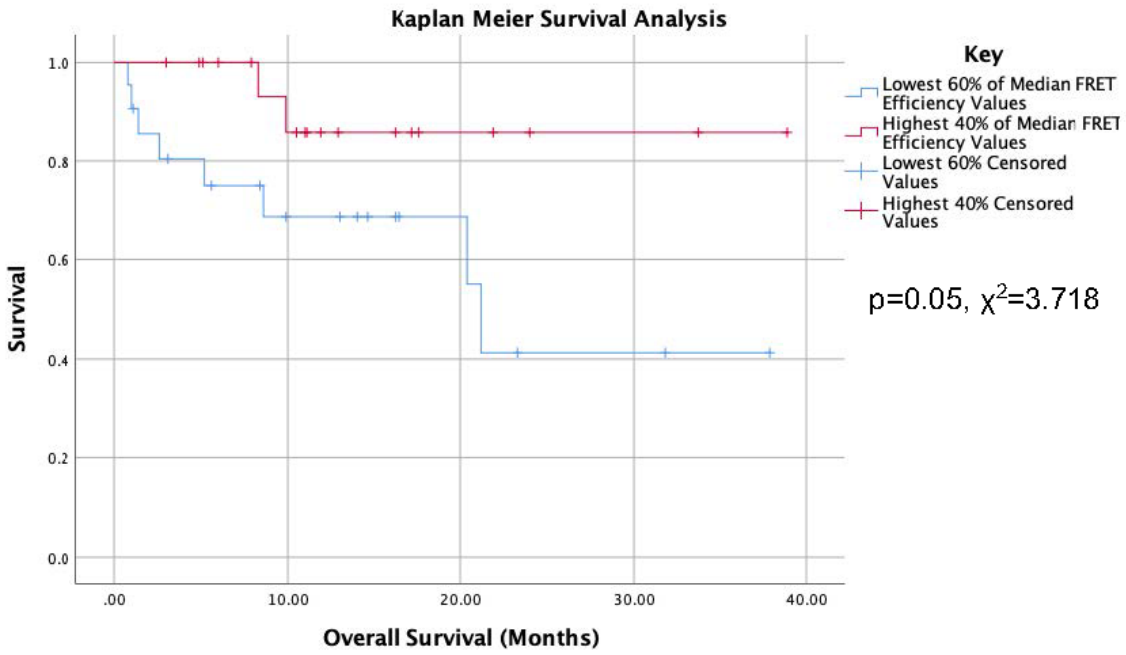

B